International Journal of
Nanoscience and Nanotechnology

Research Article 2025, Volume 21, Issue 2

Investigating the Morphological and Functional Group Characteristics of Sol-Gel Synthesized Silica Nanoparticles Derived from Natural and Commercial Precursors

Syukur Daulay[1,2], Akhmad Herman Yuwono[1,2,3*], Gusaimas M. H. H Akbar[1,2], Fairuz Septiningrum[1,2], Donanta Dhaneswara[1,2], Nofrijon Sofyan[1,2], Danang Pamungkas Priambodo[3], Agus Ismail[4]

Received 19 February 2025
Accepted 15 May 2025

DOI: 10.22034/ijnn.2026.2053759.2634

International Journal of Nanoscience and Nanotechnology

Abstract

Silica nanoparticles (SNPs) are widely investigated in scientific research and largely utilized in various functional applications. Owing to the abundant source of silica in the beach sand, there is a potential to obtain naturally derived SNPs comparable to those synthesized from commercial precursors. Therefore, this research aimed to investigate the effectiveness of the sol-gel method to produce SNPs from locally sourced silica beach sand. The synthesized SNPs were characterized using X-Ray Diffraction (XRD), Fourier Transform Infrared (FTIR) spectroscopy, and Scanning Electron Microscopy (SEM). For comparison purposes, the sol-gel process was also carried out with commercial sodium silicate and tetraethyl orthosilicate (TEOS) precursors to obtain synthetic SNPs, which were used as the standard. The FTIR spectra showed that the synthetic and fabricated SNPs exhibited a typical silica peak at a wavenumber of 950 cm^{-1}, while XRD analysis showed a diffraction peak at $2\theta = 22.05°$, characteristic of silica nanoparticles. Several additional peaks associated with ~~to~~ the quartz phase were observed at 31.96° and 43.22° for SNPs produced from natural and commercial sodium silicate. The crystallite size estimation through Scherrer's equation yielded values of 19.84, 4.40, 4.31, and 2.94 nm for SNPs synthesized from beach sand, commercial sodium silicate, TEOS, and as-received commercial SNPs, respectively. Microstructural analysis through SEM revealed a uniform particle distribution in SNPs synthesized from silica beach sand and TEOS, whereas SNPs produced from commercial sodium silicate exhibited inhomogeneous particle distribution. This investigation revealed that SNPs produced from natural beach sand are comparable to its commercial counterparts in terms of crystal structure and morphological uniformity.

Keywords: Silica nanoparticles; Sol-gel synthesis; Silica beach sand; Sodium silicate; TEOS

How to cite this article

Daulay S, Yuwono AH, Akbar GMHH, Septiningrum F, Dhaneswara D, Sofyan N, Priambodo DP, Ismail A. Investigating the Morphological and Functional Group Characteristics of Sol-Gel Synthesized Silica Nanoparticles Derived from Natural and Commercial Precursors. Int. J. Nanosci. Nanotechnol., 2025;2: 77-87. DOI: 10.22034/ijnn.2026.2053759.2634

1. Introduction

Silica nanoparticles (SNPs) are widely recognized for their promising applications in both research and industry due to the ease of the synthesis process, stable colloidal properties, adjustable particle size, biocompatibility, and scalability for large-scale production. SNPs have been widely used for several applications, ranging from drug carriers to anti-reflective coatings [1-3]. Moreover, SNPs have the potential to enhance the durability of critical infrastructure, including buildings, by providing greater mechanical and chemical stability, thereby ensuring longevity [4, 5].

Generally, nanomaterials are produced through bottom-up and top-down processes [6]. Nanoparticles are formed from the ground up by arranging atoms or molecules in the bottom-up method, while the top-down method reduces bigger particles to nano-scale dimensions. Specifically, both methods can be achieved using chemical or physical methodologies. Chemical routes involving the compositional change of specific precursors into new products include methods such as sol-gel, reverse microemulsion, and chemical vapor decomposition [7-9]. In contrast, physical routes, which involve physical changes without altering the composition, include processes such as milling, molecular condensation, physical vapor deposition, and laser ablation [10].

[1] *Department of Metallurgical and Materials Engineering-Faculty of Engineering Universitas Indonesia, Depok, West Java, Indonesia.*

[2] *Advanced Materials Research Center-Faculty of Engineering Universitas Indonesia, Depok, West Java, Indonesia*

[3] *Energy Transition Laboratory, Interdisciplinary Engineering Research Unit-Faculty of Engineering Universitas Indonesia, Depok, West Java, Indonesia*

[4] *Department of Industrial Engineering-Universitas Mercu Buana, Jakarta, Indonesia*

[*] *E-mail: ahyuwono@eng.ui.ac.id*

Among various synthesis procedures, the sol-gel process is considered ~~to be~~ the most reliable method for ~~in~~ producing SNPs. This process is a polymerization reaction, comprising the solution and ~~the~~ gel phases, which involves two important stages: hydrolysis and condensation [11, 12]. The sol-gel method offers significant advantages due to its cost-effectiveness and low processing temperature that allows for the synthesis of SNPs with high purity and uniformity [13]. Commercially, sol-gel-derived SNPs are primarily synthesized from alkoxide-based precursors, with tetraethyl orthosilicate (TEOS) being widely used [14, 15].

However, the sol-gel method still has several drawbacks, such as expensive precursors and long processing time. These concerns have been discussed in previous studies [16-18], highlighting the necessity to procure affordable materials and shorter synthesis durations. Therefore, a combination of limited sources and time-consuming production processes remains a challenge to meet the global demand for ~~of~~ SNPs.

In recent times, there has been a growing interest in exploring natural sources of raw materials such as rice husks, clay, palm oil shells, and beach sand [19, 20]. This process of using natural precursors includes the extraction of silica, followed by the conversion of silica into sodium silicate (Na_2SiO_3), which is used to produce SNPs through the sol-gel method [20, 21]. Arunmetha et al. [22] investigated the synthesis SNPs derived from natural beach sand and conducted a comparative analysis of chemical and physical synthesis methods. The study found that chemical methods produced SNPs with larger particle sizes, lower surface area, and lower bandgap. Another investigation by El-Didamony et al. [23] fabricated SNPs from commercial sodium silicate commonly used in the production of traditional ceramics. The SNPs improved the physico-chemical properties of the ceramic, such as thermal expansion, water absorption, and crystallinity. M.S. Hamzah et al. [24] synthesized SNPs from silica sand using a vibration-assisted alkaline solution method and showed that the size of SNPs decreased as the vibration frequency increased.

Previous studies have employed diverse approaches to synthesize SNPs from natural and commercial precursors. However, these investigations predominantly focus on utilizing a single method and a single precursor. Despite advancements in synthesis methods, there remains a lack of comparative evaluation of SNPs produced from natural and commercial sources. Therefore, this research aims to bridge this gap by conducting a comparative analysis of the morphological and chemical properties of sol-gel-derived SNPs synthesized from silica beach sand and those produced from commercial precursors, such as sodium silicate, TEOS, and as-received commercial SNPs. Moreover, this study characterized and compared the chemical behavior of each precursor, as well as its intermediate products, in the synthesis of SNPs. This research exemplifies the application of sol-gel methods utilizing cost-effective reactants.

2. Materials and Methods

2.1. Materials

Silica beach sand sourced from Belitung Island, Indonesia, was used as a natural precursor for the synthesis of SNPs via the sol-gel method. SNPs were also synthesized using commercial precursors, including tetraethyl orthosilicate (TEOS) and sodium silicate (Na_2SiO_3), obtained from Sigma-Aldrich. Other chemicals used in the sol-gel synthesis, such as sodium hydroxide (NaOH), 37% hydrochloric acid (HCl), and 25% ammonia (NH_3), were commercially purchased from MERCK. The SNPs produced from synthesized and commercial precursors were further compared with commercially available ultrapure 99% silicon dioxide (SiO_2) nanoparticles obtained from XFNANO Ltd, and denoted as **SNPXFNANO.**

2.2. Synthesis of SNPs from Beach Sand

Belitung beach sand with a 325-mesh sieve was mixed with 8 M NaOH solution, producing a mixture composed of 250 mL of distilled water, 64 g of silica beach sand, and 48 g of NaOH at a temperature of 90°C. This mixture was stirred with a magnetic stirrer for 2 hr. Subsequently, the solution was filtered using Whatman filter paper to obtain the sodium silicate solution filtrate, which was denoted as **SSN**. Afterward, 50 mL of the obtained SSN solution was mixed with 50 mL of ethanol (99% purity, MERCK), and 3 M HCl was slowly added dropwise until a pH of 7 was achieved. The mixture was left for 5 days, followed by washing and drying at room temperature, which was denoted as **SNPNRT**. This sample was dried again at a temperature of 100°C for 30 min, followed by calcination at 600°C for 2 h, and denoted as **SNPN600**.

2.3. Synthesis of SNPs from Commercial Sodium Silicate

A commercial solution of sodium silicate (10 mL) was mixed with distilled water (90 mL) and to form **SSC**. Subsequently, 3 mL of 3 M HCl solution was added dropwise until a neutral pH was obtained. Then, the solution was left for 5 days, followed by crushing and drying at 100°C for 30 min and calcination at 600°C for 2 h. SNPs produced using commercial sodium silicate were denoted as **SNPC600**.

2.4. Synthesis of SNPs from TEOS

TEOS was mixed with ethanol in an 8:12 ml ratio and stirred at a speed of 400 rpm for 30 min. NH_3 solution (5:5 ml) was added dropwise at 60°C for 45 min, until the solution turned white. The solution was left for 5 days, dried at 100°C for 30 min, followed by calcination at 600°C for 2 h. SNPs produced using the commercial TEOS precursor were denoted as **SNPTEHN600**.

2.5 Characterizations

Several characterization techniques were used to investigate the properties of the synthesized SNPs. X-ray fluorescence (XRF) spectroscopy was used to determine the elemental composition of the beach sand precursor, while X-ray diffraction (XRD) was performed to analyze the

phase and crystallographic properties. The crystallite size of the samples was calculated using Scherrer's equation as shown in Equation 1[25] :

$$D = \frac{K\lambda}{\beta \cos\theta} \quad (1)$$

where D is crystallite size, $K = 0.9$ is Scherrer's constant, λ is the wavelength, β is full width at half maximum (FWHM), and ϑ is the Bragg angle.

Fourier Transform Infrared (FTIR) spectroscopy was used to determine the functional groups present in the intermediate products and SNPs. To complement chemical analysis from FTIR spectroscopy, X-ray photoelectron spectroscopy (XPS) was also employed. Furthermore, Scanning Electron Microscopy and Energy Dispersive Spectroscopy (SEM-EDX) were used to investigate morphology and elemental composition.

3. Results and Discussion

This study investigates the properties of SNPs synthesized from a natural-derived silica precursor, and compares them with those prepared using commercial precursors, including sodium silicate and TEOS.

3.1. Silica Beach Sand Characteristics

The X-ray diffractogram of silica beach sand precursor in Figure 1 showed dominant peaks appearing at 2θ values of 20.85°, 26.63°, and 50.12° [26, 27]. Crystallographic analysis using X'pert HighScore Plus software determined that the peaks in the diffractogram pattern corresponded to the quartz database (01-085-0930) [28, 29]. The crystallographic calculation results determined a hexagonal crystal structure with values a = b = 4.9115 Å, c = 5.4038 Å, along with angles α = β = 90° and γ = 120°. Furthermore, the crystallite size of the natural precursor was calculated through Scherrer's equation and determined to be 75.73 nm.

XRF analysis showed that the beach sand precursor was primarily composed of silica (SiO_2), containing 96.40%, while other components of significance included Al_2O_3 (1.19%) and MgO (1.54%). Additional compounds such as CaO, SO_3, ZrO_2, and P_4O_6, are 0.09, 0.15, 0.12, and 0.44 %, respectively. These XRD and XRF analyses confirmed that the primary constituent of the beach sand was silica.

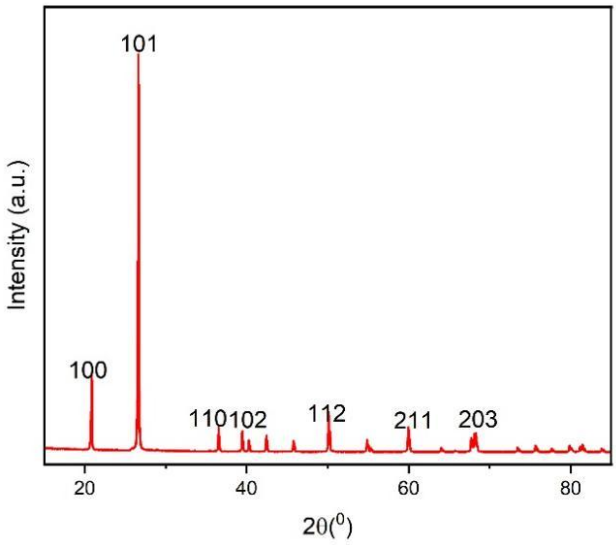

Figure 1. X-ray diffraction pattern of silica beach sand.

The morphology of silica beach sand was investigated using SEM, with the micrographs (Figures 2a and 2b) at 1000× and 5000× magnifications. Visual examination of the SEM results showed that the silica beach sand is dominated by large aggregates accompanied with fine flake-like particles. Further quantitative analysis using ImageJ analysis determined that the average particle size (x) was 4.78 µm with a standard deviation (σ) of 3.02 µm. The considerable magnitude of the standard deviation indicated a broad particle size distribution and inhomogeneity.

Elemental analysis was examined using EDX to obtain the chemical composition of the silica beach sand. Figure 2c showed high-intensity peaks that are characteristic from silicon and oxygen. Table 1 provides details on atomic percentage and weight percentage. Stoichiometric calculations showed the weight ratio of silicon to oxygen is approximately 7:8, derived from their respective atomic masses of 28 and 32. The atomic ratio is 1:2, reflecting the composition of SiO_2, which consists of one silicon atom and two oxygen atoms.

3.2. Functional Group of SNPs

3.2.1. SNPs from Silica Sand

Chemical analysis using FTIR spectroscopy were performed on four samples of silica beach sand, SSN, SNPNRT, and SNPN600, and the result is shown in Figure 3. Specifically, Figure 3a shows the spectrum of silica beach sand with a peak at 1060 cm^{-1}, which corresponds to asymmetric stretching vibrations of Si-O-Si bonds. Additionally, peaks observed at 950 and 472 cm^{-1} were attributed to the bending vibrations and symmetric stretching of Si-O-Si bonds, respectively [30].

After NaOH digestion, the peaks corresponding to the Si-O-Si bonds (950, and 1060 cm^{-1}) showed significant changes, indicating the conversion of silica into sodium silicate as shown in Figure 3b. A strong and broad peak was observed at 3400 cm^{-1} and a smaller peak at 1620 cm^{-1} correspond to the stretching and bending vibrations of hydroxyl (-OH) groups, respectively. This observed change in the functional group was caused by a chemical reaction between silica and NaOH (Equation 2) [22]:

$$SiO_{2(s)} + NaOH_{(aq)} \rightarrow Na_2SiO_{3(aq)} + H_2O_{(l)} \quad (2)$$

According to Okunev et al. [31, 32], during NaOH digestion of silica, hydroxide ions (OH-) from NaOH interact with the Si-O-Si bonds in the silica network, weakening the Si-O bonds. This chemical process results in the formation of SiO_3^{-2} anions, which subsequently bond with Na^+ ions to produce sodium silicate [33-36].

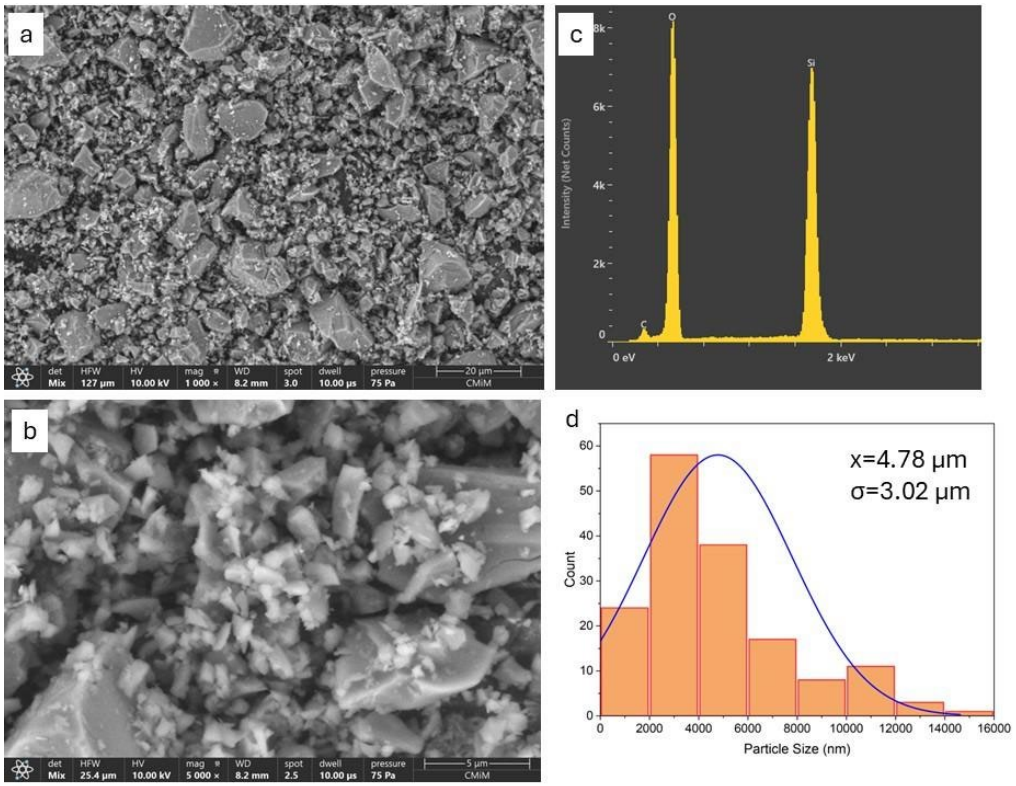

Figure 2. SEM of silica beach sand with magnifications of (a) 1000× X and (b) 5000×X, (c) EDS spectrum, and (d) particle size distributio

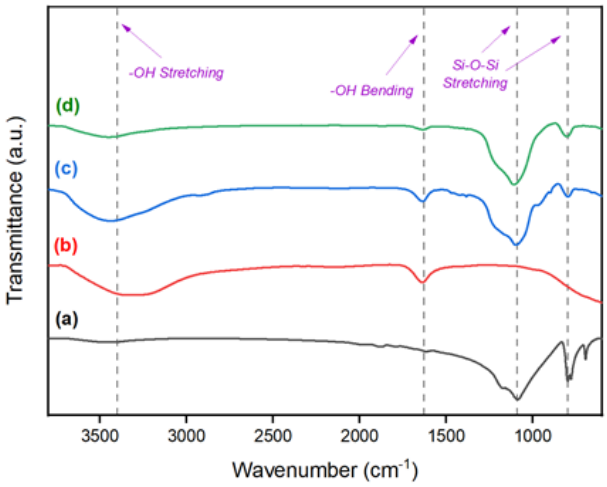

Figure 3. FTIR spectra of (a) silica beach sand, (b) SSN, (c) SNPNRT, and (d) SNPN600

During the sol-gel process, HCl was added dropwise into the alkaline sodium silicate solution. This caused an acid-base neutralization reaction which was reflected by the reduction in the hydroxyl (-OH) group, as shown by diminished peaks in the FTIR spectra at 3400 cm^{-1} and 1620 cm^{-1} [30, 37, 38]. The hydroxyl peaks were further diminished after room temperature drying, as shown in Figure 3c, and eliminated after calcination at 600°C (Figure 3d). Peaks associated with Si-O-Si bonds were regenerated for SNPNRT and SNPN600 samples, indicating the successful formation of silica.

The chemical reaction between sodium silicate and HCl led to the formation of sodium chloride (NaCl) and silicic acid (H_2SiO_3 or $SiO_2.H_2O$) through the replacement of Na^+ ions by H^+ ions [39]. During this reaction, silicic acid molecules created long chains of molecules through condensation [40]. Further drying process along with calcination led to the decomposition of H_2SiO_3, causing the separation of silica and water, thereby producing SNPs. The chemical reactions of aforementioned processes are summarized in Equations 3 and 4 [39, 40]:

Table 1. Atomic and weight percentages of the elemental analysis

Element	Atomic %	Weight %
C	4.9	3
O	62	50.1
Si	33.1	46.9

$$Na_2SiO_{3(aq)} + 2HCl_{(aq)} \rightarrow H_2SiO_{3(s)} + 2NaCl_{(aq)} \quad (3)$$

$$H_2SiO_{3(s)} \rightarrow SiO_{2(s)} + H_2O_{(l)} \quad (4)$$

3.2.2. SNPs from Commercial Sodium Silicate

The infrared analysis presented in Figure 4 was conducted on commercial sodium silicate (SSC) solution and its synthesized product (SNPC600). The spectra showed that both samples exhibit a peak at approximately 3500 cm^{-1}, which corresponds to hydroxyl (-OH) group's vibration. Additionally, a peak at 1060 cm^{-1} corresponding to the asymmetric stretching of Si-O-Si bonds was observed in SNPC600 and not in SSC [41]. FTIR analysis indicated

that the sol-gel method, combined with the drying and calcination process, has successfully produced SNPs.

The spectra for SSN and SSC (Figures 4a and 4b) exhibited similar functional groups, including a prominent hydroxyl group in the 3400-3500 cm^{-1} range. The SNPs derived from both SSN and SSC showed the same peak at 1060 cm^{-1} that corresponds to Si-O-Si bonds [4]. This suggests that the functional groups of sodium silicate and SNPs derived from natural sources are comparable with those commercially used.

3.2.3. SNPs synthesized from TEOS

In addition to sodium silicate, TEOS ($Si(OC_2H_5)_4$) was used as a commercial precursor for further comparison. Chemical analysis was performed on the TEOS solution using infrared spectroscopy as presented in Figure 5a, showing peaks associated with Si-O-Si vibrations, symmetric and asymmetric stretching (950 and 1060 cm^{-1}). Additionally, peaks in the 2900 cm^{-1} region associated with C-H stretching vibrations were also observed [42].

Following the sol-gel process and calcination, three peaks associated with Si-O-Si asymmetric stretching at 900-1200 cm^{-1} found in TEOS spectrum were converted into a single broad peak in the final SNPs (SNPTEHN600) as shown in Figure 5b [43, 44].

During the sol-gel process, TEOS underwent hydrolysis in an alkaline environment, forming silanol groups. Subsequently, silanol groups undergoes a polycondensation reaction that generates Si-O-Si linkages and water [45].

3.2.4. Comparison of Synthesized and As-Received Commercial SNPs

SNPs synthesized from both natural and commercial precursors were compared with as-received commercial SNPs (SNPXFNANO). Figure 6 depicts the FTIR spectra of all four types of SNPs produced using natural and commercial precursors, compared with the as-received SNPs. Peaks are assigned to the asymmetric stretching of the Si-O-Si bonds at 1060 cm^{-1}. An additional peak at 950 cm^{-1} was attributed to symmetric stretching vibrations associated with SNPs [41]. This functional group analysis strongly suggested that the functional groups profiles of the synthesized SNPs from both natural and commercial precursors were comparable to those of as-received commercial SNPs.

3.3. Phase and Crystallite Size of SNPs

The XRD diffraction patterns of SNPs synthesized using natural and commercial precursors, as well as SNPXFNANO, are shown in Figure 7. All samples exhibited a broad peak at a 2θ angle of approximately 22.05°, which

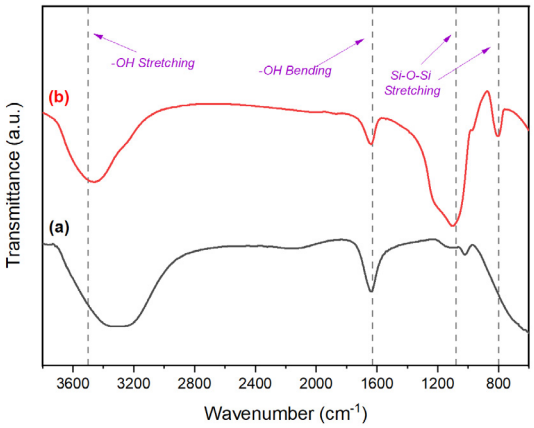

Figure 4. FTIR spectra for (a) SSN and (b) SSC

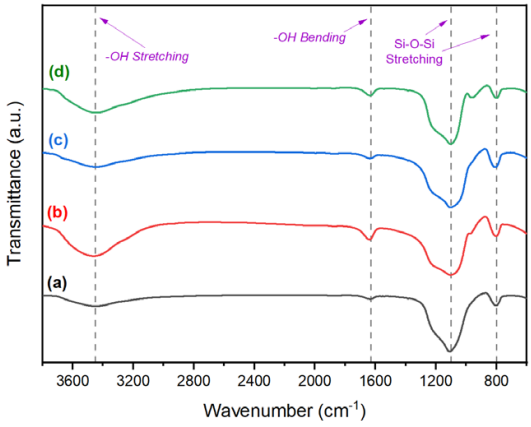

Figure 5. FTIR spectra for (a) TEOS and (b) SNPTEHN600

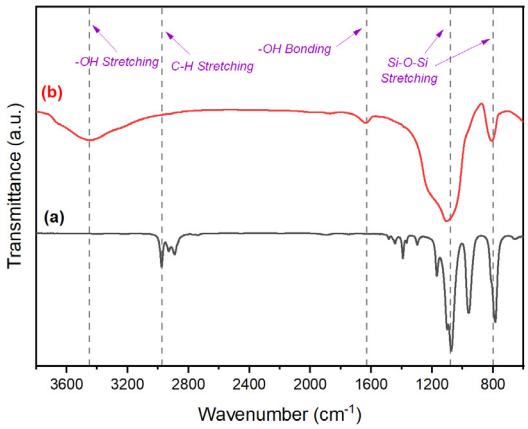

Figure 6. FTIR spectra for (a) SNPN600, (b) SNPC600, (c) SNPTEHN600, and (d) SNPXFNANO

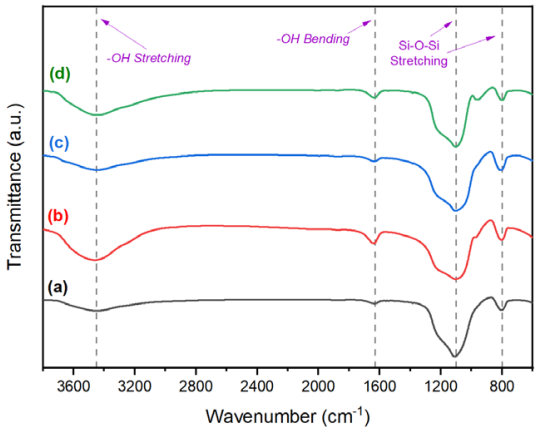

Figure 7. XRD pattern for (a) SNPN600, (b) SNPC600, (c) SNPTEHN600, and (d) SNPXFNANO

is the characteristic of silica quartz (SiO_2) crystal structure for the (100) planes [46]. Additionally, the crystallite size estimated using the Scherrer equation were 19.84, 4.40, 4.31, and 2.94 nm for SNPN600, SNPC600, SNPTEHN600, and XFNANO, respectively.

Notably, SNPs synthesized from silica beach sand and commercial sodium silicate showed significantly weaker peaks at 22.05° (Figures 7a and 7b). Additional peaks were also observed in SNPC600 samples (Figure 7b) that corresponded to the diffraction pattern of sodium silicate hydrate ($Na_2SiO_3.5H_2O$) (JCPDS 00-003-0433)[47]. The presence of these peaks indicates incomplete conversion of the precursor material into SNPs. Residual (unreacted) sodium silicate, which can form hydrated phases during processing, likely explains the distinct peaks in the SNPC600 diffractogram [48].

3.4. Microstructure and Particle Size of SNPs

SEM was performed to further characterize the morphology and particle size distribution of SNPs. Figure 8 depicts the micrographs at 5000× and 10,000× magnifications. SNPN600 (Figure 8a and 8b) and SNPTEHN600 (Figure 8e and 8f) both exhibit spherical nanoparticles that are uniformly distributed and non-

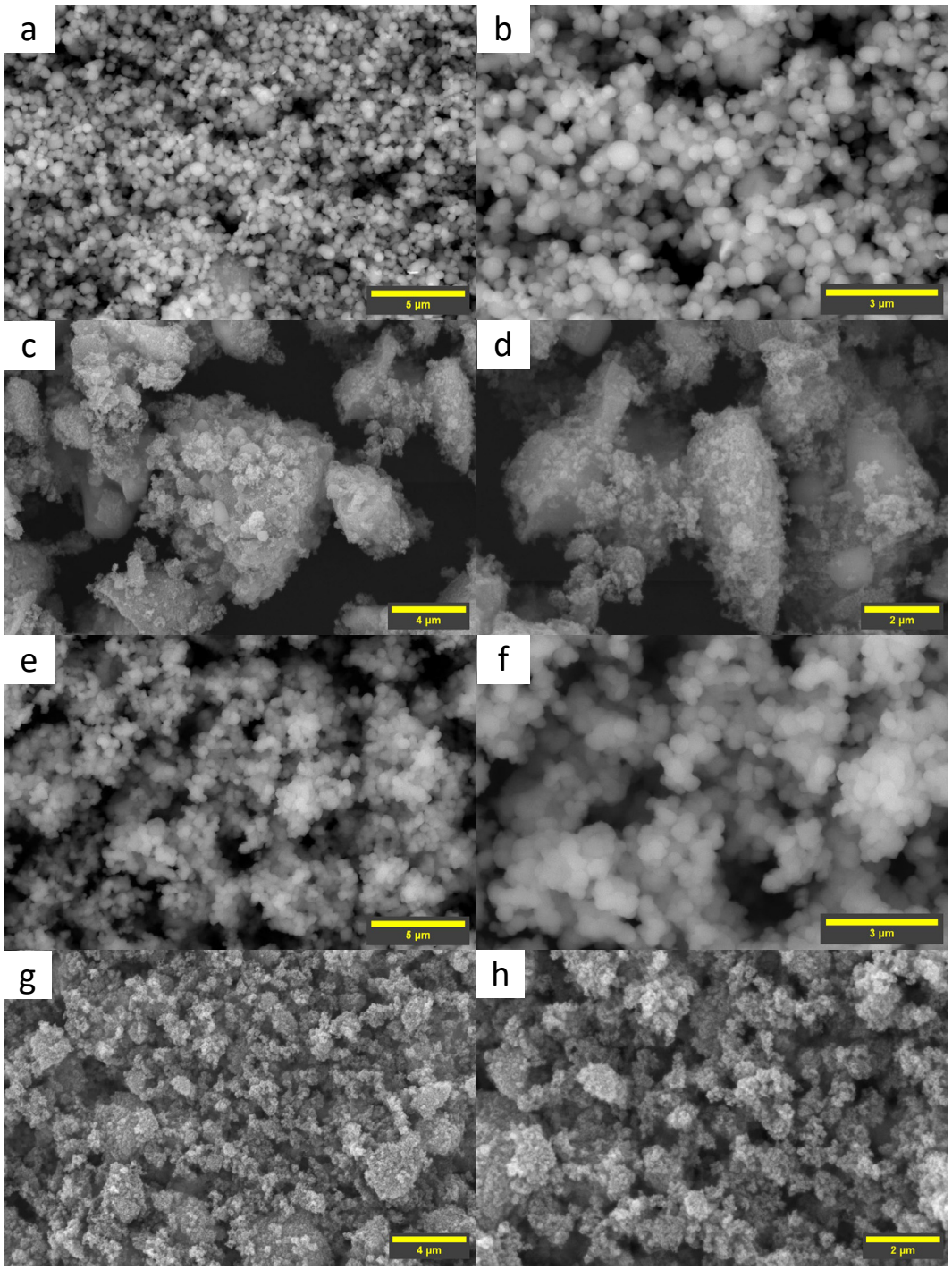

Figure 8. SEM images of (a, b) SNPN600, (c, d) SNPC600, (e, f) SNPTEHN600, and (g, h) SNPXFNANO with magnifications of 5000× and 10,000×

agglomerated. Notably, the SNPs produced by processing silica beach sand closely resemble those synthesized using TEOS, which is the primary commercial precursor used to produce SNPs.

The micrograph for SNPC600 in Figure 8c-d shows irregularly shaped particles, accompanied by small spherical formations on their exteriors. These particles are presumed to be sodium hydrate, accompanied by partially formed SNPs on its surface. In comparison, SNPXFNANO exhibited small nanoparticles that were visibly agglomerated, as a consequence of their very fine particle size leading to high surface energy, as shown in Figure 8g-h.

To complement the morphological evaluation conducted via SEM, particle size analysis and distribution were performed for all SNPs, as shown in Figure 9. The average particle sizes, from smallest to largest, were as follows: SNPXFNANO (128.64 ± 43.67 nm), SNPC600 (258.54 ± 186.92 nm), SNPTEHN600 (360.77 ± 101.38 nm) and SNPN600 (371.05 ± 126.80 nm). Furthermore, the coefficient of variation, calculated by dividing the standard deviation by the mean particle size [49], indicated that SNPC600 exhibited the highest the highest particle size variability (72.29%), whereas SNPTEHN600 showed the lowest variability (28.10%). By comparison, the coefficient of variation of SNPN600 was 34.17%, indicating a relatively homogeneous particle size.

The morphological differences observed in SNPs synthesized from natural and commercial precursors are likely attributed to variations in silicate concentration, which significantly influenced the reaction kinetics and formation of particles [50, 51]. Additional studies have also reported that the synthesis parameters and the concentration of reagents, such as ethanol and ammonia, during the sol-gel process play a crucial role in the size and distribution of SNPs [52, 53]. The irregular particles identified in SNPC600 are thought to result from imbalanced hydrolysis and condensation rates during the reaction. Consequently, it is hypothesized that the SNPs produced from commercial sodium silicate were partially formed on the surfaces of unreacted, irregularly shaped sodium silicate hydrate particles, as evidenced by electron microscopy and XRD analysis. In comparison, TEOS showed significantly different results as the silanol group gradually reacted and converted into SNPs in the presence of ethanol and NH_3 [50]. Through this mechanism, spherical and nano-sized silica particles were successfully formed and observed in the electron micrograph.

3.5. Investigation of Surface Chemistry Using XPS

A comprehensive XPS analysis was conducted to complement infrared spectroscopy, with the full survey spectra of silica beach sand, SSN, and SSC presented

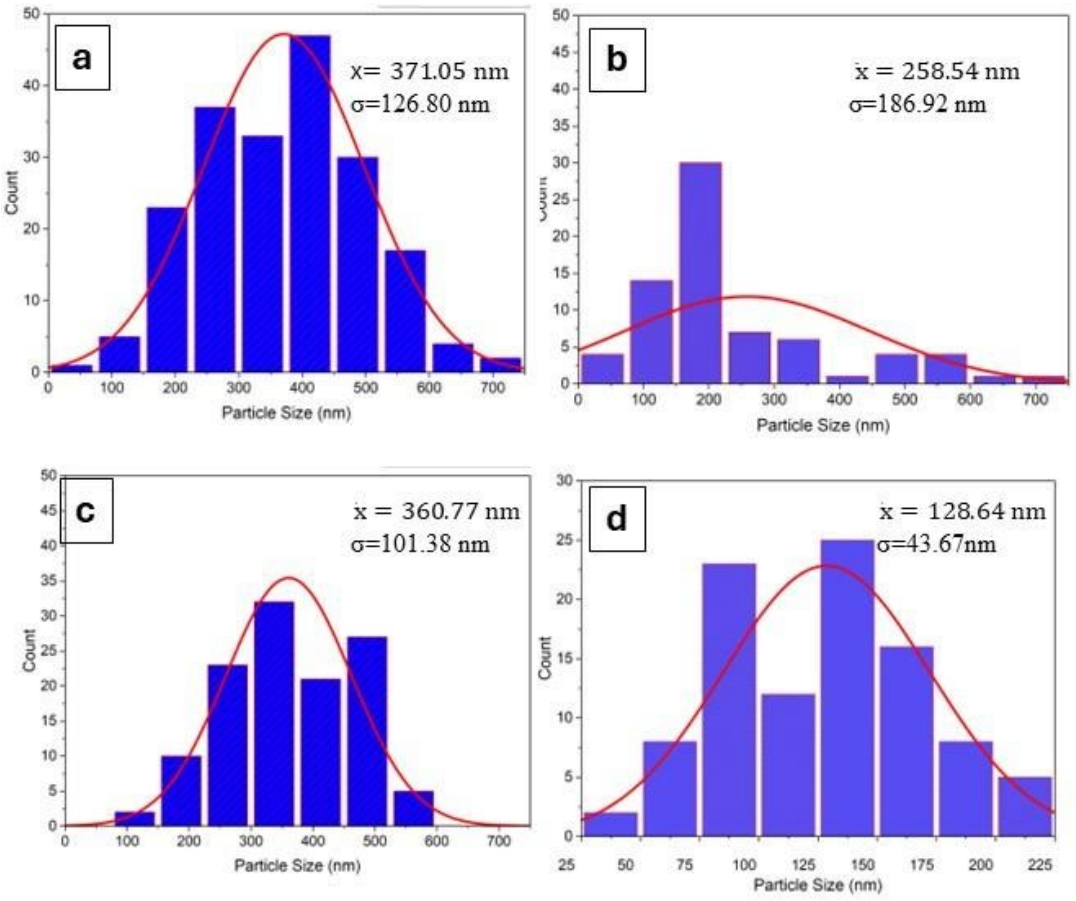

Figure 9. Particle size distribution of (a) SNPN600, (b) SNPC600, (c) SNPTEHN600 and (d) SNPXFNANO

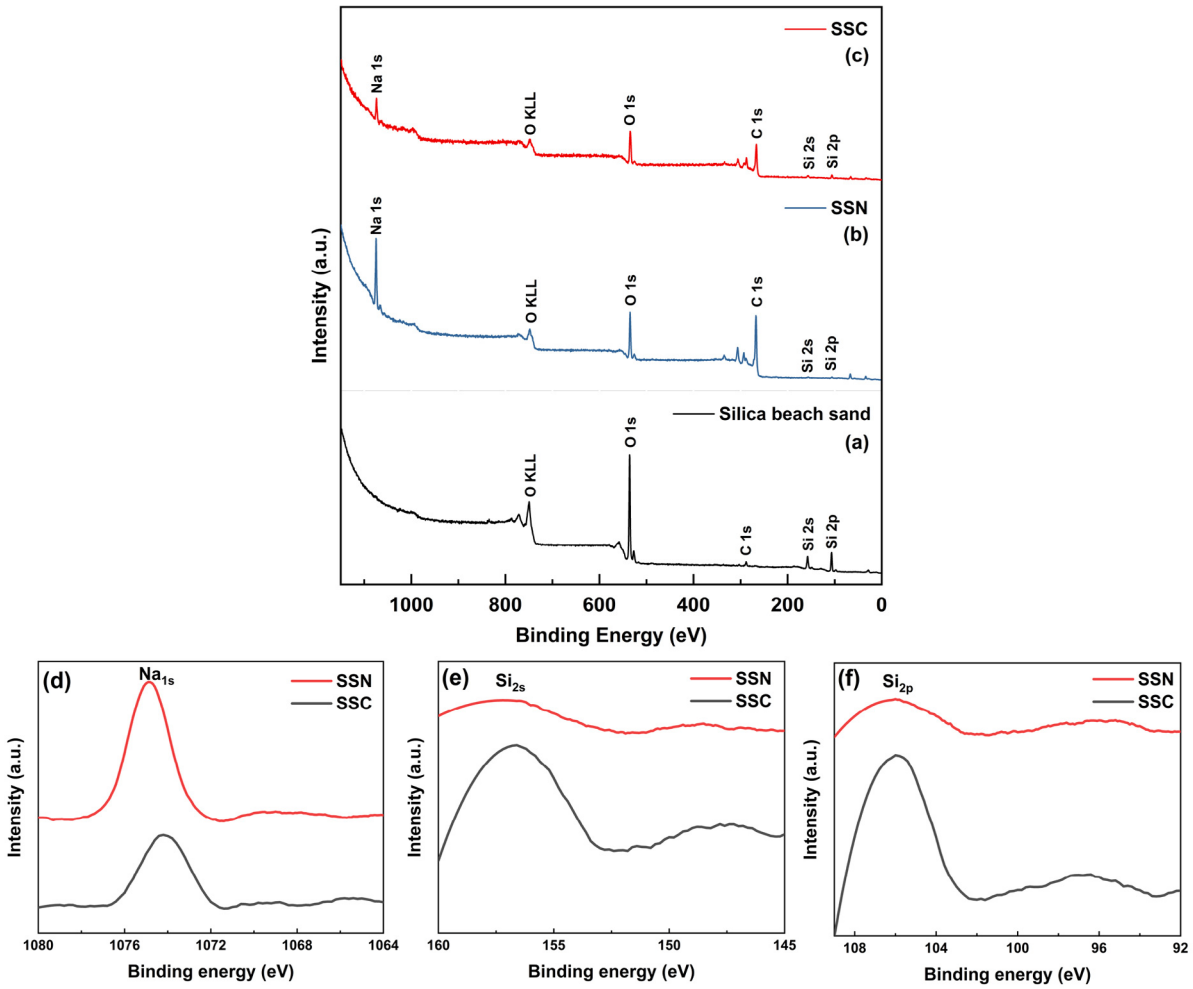

Figure 10. XPS Scanning Spectra for: full survey of (a) silica beach sand, (b) SSN, (c) SSC, and the narrow scan for (d) Na1s, (e) Si2s, (f) Si2p core-level

in Figures 10a, b, and c. The electron core-levels corresponding to Si_{2s}, Si_{2p}, O_{1s}, O_{KLL}, and C_{1s} in the spectra confirms the presence of silicon and oxygen components across all samples.

The detection of Na_{1s} core levels in SSN (1074.8 eV) and SSC (1074.1 eV) as observed in Figure 10d indicates the presence of sodium. Furthermore, electrons from the 2s and 2p orbitals of silicon were also comfirmed in SSN and SSC, as shown in Figures 10e and 10f. The Si_{2s} peak, appearing around 150-160 eV, and the Si_{2p} peak, around 102-108 eV (Figures 10e and 10f) [22, 54]. This investigation confirms that the digestion process of silica beach sand with NaOH successfully produced Na_2SiO_3 [55], which also affirms what has been studied using FTIR in the previous section.

A full XPS survey was also performed on the SNPs produced from natural and commercial precursors. SNPs derived from commercial TEOS (SNPTEHN600) were selected for comparison with those from silica beach sand, as FTIR analysis revealed similar functional groups, while SEM morphology showed uniformly distributed, non-agglomerated particles. The full XPS survey showed the presence of silicon and oxygen, evidenced by the peaks corresponding to the electron core-levels for Si_{2s}, Si_{2p}, O_{1s}, O_{KLL}, and C_{1s}. Notably, the Si_{2p} peak at 106.4 eV is characteristic of pure SiO_2 [56] while the binding energy around 535.7 eV is attributed to the electron of O_{1s} [57]. The binding energy of O_{1s} is attributed to the siloxane (Si-O-Si) and silanol (Si-O-H) groups, in agreement with ~~to~~ the XPS investigation performed by Tang et al. [58, 59].

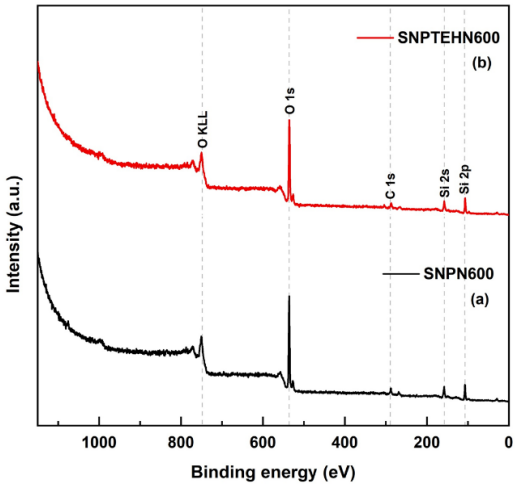

Figure 11. Full Survey XPS Spectra for (a) SSN and (b) SNPTEHN600

4. Conclusion

This research showed that SNPs using silica beach sand as a natural precursor were successfully produced through the sol-gel method. FTIR analysis showed that the synthesized SNPs have the peak at ~~of~~ 950 cm^{-1}, which corresponds to Si-O-Si bonds, which are a typical characteristic of the SiO_2 quartz phase. XPS analysis further confirmed the successful conversion of silica beach sand into sodium silicate as well as the formation of SNPs comparable to those produced from commercial precursors. Additionally, crystal structure analysis by XRD analysis confirmed that the diffraction peak at a 2θ angle of 22.05° belongs to the silica phase in SNPs. Such results were comparable to those reported in previous studies on SNPs derived from commercial precursors.

Microstructural and particle size analysis by SEM show that SNPs synthesized from natural silica beach sand demonstrated a uniform distribution which is comparable to that derived from TEOS, although its average size is rather larger than that of particles derived from TEOS. By contrast, agglomeration was observed in SNPs obtained from commercial sodium silicate precursors.

While the characterization of the synthesized SNPs revealed that the obtained results from silica beach sand showed promising morphology and properties, further development is still required for this approach to compete with established SNPs in terms of industrial-scale production.

Acknowledgement

This research was funded by the Center for Higher Education Fund (*Balai Pembiayaan Pendidikan Tinggi*), Ministry of Education, Culture, Research, and Technology of Indonesia, based on the decision letter of the Head of Education Funding Service Center with number of 0831/J5.2.3./BPI.06/10/2021.

Conflict of interest

The authors declare that there is no conflict of interest that could have influenced the results reported in this paper.

References

1. Xu Y, Yang Y, Fan X, Liu Z, Song Y, Wang Y, et al. In-situ silica nanoparticle assembly technique to develop an omniphobic membrane for durable membrane distillation. Desalination. 2021;499:114832. https://doi.org/10.1016/j.desal.2020.114832
2. Li T, Shi S, Goel S, Shen X, Xie X, Chen Z, et al. Recent advancements in mesoporous silica nanoparticles towards therapeutic applications for cancer. Acta Biomater. 2019;89:1-13. https://doi.org/10.1016/j.actbio.2019.02.031
3. Zhou G, He J. Antireflective Coatings on Fresnel Lenses by Spin-Coating of Solid Silica Nanoparticles. J Nanosci Nanotechnol. 2013;13(8):5534-5541. https://doi.org/10.1166/jnn.2013.7480
4. Basnet S, Shah S, Joshi R, Pandit R. Investigation of Compressive Strength of Cement/Silica Nanocomposite Using Synthesized Silica Nanoparticles from Sugarcane Bagasse Ash. Int J Nanosci Nanotechnol. 2022;18(2):93-98.
5. Oh YJ, Song H, Shin WS, Choi SJ, Kim YH. Effect of amorphous silica and silica sand on removal of chromium(VI) by zero-valent iron. Chemosphere. 2007;66(5):858-865. https://doi.org/10.1016/j.chemosphere.2006.06.034
6. Gratowski S von, Koledov V. 3D mechanical bottom up nano-manipulation and nano-assembling using shape memory alloy nanogripper for nano-optic, nano-photonics, nano-plasmonics. J Phys Conf Ser. 2020;1461:012186. https://doi.org/10.1088/1742-6596/1461/1/012186
7. Karande S, Jadhav S, Garud H, Kalantre V, Burungale S, Patil P. Green and sustainable synthesis of silica nanoparticles. Nanotechnol Environ Eng. 2021;6(2):31. https://doi.org/10.1007/s41204-021-00124-1
8. Lin CH, Chang JH, Yeh YQ, Wu SH, Liu YH, Mou CY. Formation of hollow silica nanospheres by reverse microemulsion. Nanoscale. 2015;7(21):9614-9626. https://doi.org/10.1039/C5NR01395J
9. Yue R, Meng D, Ni Y, Jia Y, Liu G, Yang J, et al. One-step flame synthesis of hydrophobic silica nanoparticles. Powder Technol. 2013;235:909-913. https://doi.org/10.1016/j.powtec.2012.10.021
10. Al-Harbi N, Abd-Elrahman NK. Physical methods for preparation of nanomaterials, their characterization and applications: a review. J Umm Al-Qura Univ Appl Sci. 2024;10(4):615-631.
11. Karim A, Ali A, Mezan S. Synthesis and Characterization of Silica Nanoparticle (SiO2 NPs) Via Chemical Process. Ann Rom Soc Cell Biol. 2021;25(6):6211-6218.
12. Bokov D, Turki Jalil A, Chupradit S, Suksatan W, Javed Ansari M, Shewael IH, et al. Nanomaterial by Sol-Gel Method: Synthesis and Application. Adv Mater Sci Eng. 2021;2021:5102014. https://doi.org/10.1155/2021/5102014
13. Modan M, Schiopu AG. Advantages and Disadvantages of Chemical Methods in the Elaboration of Nanomaterials. Mod Sci Mater. 2020;43(1):43-52. https://doi.org/10.35219/mms.2020.1.08
14. Aboelenin RMM, Fathy NA, Farag HK, Sherief MA. Preparation, characterization and catalytic performance of mesoporous silicates derived from natural diatomite: Comparative studies. J Water Process Eng. 2017;19:112-119. https://doi.org/10.1016/j.jwpe.2017.07.017
15. Gao L, He J. A facile dip-coating approach based on three silica sols to fabrication of broadband antireflective superhydrophobic coatings. J Colloid Interface Sci. 2013;400:24-30. https://doi.org/10.1016/j.jcis.2013.03.013
16. Ibrahim NB, AL-Shomar SM, Ahmad SH. Effect of aging time on the optical, structural and photoluminescence properties of nanocrystalline ZnO films prepared by a sol-gel method. Appl Surf Sci. 2013;283:599-602. https://doi.org/10.1016/j.apsusc.2013.06.155
17. Yazıcı M, Çomaklı O, Yetim T, Yetim AF, Çelik A. Effect of sol aging time on the wear properties of TiO2-SiO2 composite films prepared by a sol-gel method. Tribol Int. 2016;104:175-182. https://doi.org/10.1016/j.triboint.2016.08.041
18. Hernández-Barrios CA, Cuao CA, Jaimes MA, Coy AE, Viejo F. Effect of the catalyst concentration, the immersion time and the aging time on the morphology, composition and corrosion performance of TEOS-GPTMS sol-gel coatings deposited on the AZ31 magnesium alloy. Surf Coat Technol. 2017;325:257-269. https://doi.org/10.1016/j.surfcoat.2017.06.047
19. Shen Y. Rice husk silica derived nanomaterials for sustainable applications. Renew Sustain Energy Rev. 2017;80:453-466. https://doi.org/10.1016/j.rser.2017.05.115
20. Hossain SKS, Mathur L, Roy PK. Rice husk/rice husk ash as an alternative source of silica in ceramics: A review. J Asian Ceram Soc. 2018;6(4):299-313. https://doi.org/10.1080/21870764.20

18.1539210
21. Usgodaarachchi L, Thambiliyagodage C, Wijesekera R, Bakker MG. Synthesis of mesoporous silica nanoparticles derived from rice husk and surface-controlled amine functionalization for efficient adsorption of methylene blue from aqueous solution. Curr Res Green Sustain Chem. 2021;4:100116. https://doi.org/10.1016/j.crgsc.2021.100116
22. Arunmetha S, Karthik A, Srither SR, Vinoth M, Suriyaprabha R, Manivasakan P, et al. Size-dependent physicochemical properties of mesoporous nanosilica produced from natural quartz sand using three different methods. RSC Adv. 2015;5(59):47390-47397. https://doi.org/10.1039/C5RA07074K
23. El-Didamony H, El-Fadaly E, Amer AA, Abazeed IH. Synthesis and characterization of low cost nanosilica from sodium silicate solution and their applications in ceramic engobes. Bol Soc Esp Ceram Vidr. 2020;59(1):31-43. https://doi.org/10.1016/j.bsecv.2019.06.004
24. Hamzah MS, Wildan MW, Kusmono K, Suharyadi E. Synthesis of Silica Nanoparticles from Silica Sand via Vibration Assisted Alkaline Solution Method. Int J Eng. 2022;35(7):1300-1306. https://doi.org/10.5829/IJE.2022.35.07A.09
25. Sarangi M, Nayak P, Tiwari TN. Effect of temperature on nano-crystalline silica and carbon composites obtained from rice-husk ash. Compos B Eng. 2011;42(7):1994-1998. https://doi.org/10.1016/j.compositesb.2011.05.026
26. Deb Barma M, Kannan S, Indiran M, Shanmugam R, Kumar R P. Antibacterial Activity of Mouthwash Incorporated with Silica Nanoparticles against S. aureus, S. mutans, E. faecalis: An in-vitro Study. J Pharm Res Int. 2020;32(16):25-33. https://doi.org/10.9734/jpri/2020/v32i1630646
27. Hariyanto B, Wardani D, Kurniawati N, Har N, Darmawan N, Husein I. X-Ray Peak Profile Analysis of Silica by Williamson-Hall and Size-Strain Plot Methods. J Phys Conf Ser. 2021;2019:012106. https://doi.org/10.1088/1742-6596/2019/1/012106
28. Calas G, Bassett WA, Petiau J, Steinberg M, Tchoubar D, Zarka A. Some mineralogical applications of synchrotron radiation. Phys Chem Miner. 1984;11(1):17-36. https://doi.org/10.1007/BF00309373
29. Pakhnevich A, Lychagina T, Morris S, Nikolayev D. Local Crystallographic Texture of Alpha Quartz in Silicified Wood (Late Triassic, Madagascar). Minerals. 2024;14(11):1128. https://doi.org/10.3390/min14111128
30. Yan F, Jiang J, Chen X, Tian S, Li K. Synthesis and Characterization of Silica Nanoparticles Preparing by Low-Temperature Vapor-Phase Hydrolysis of SiCl4. Ind Eng Chem Res. 2014;53(29):11884-11890. https://doi.org/10.1021/ie501759w
31. Okunev AG, Shaurman SA, Danilyuk AF, Aristov YI, Bergeret G, Renouprez A. Kinetics of the SiO2 aerogel dissolution in aqueous NaOH solutions: experiment and model. J Non Cryst Solids. 1999;260(1-2):21-30. https://doi.org/10.1016/S0022-3093(99)00568-2
32. Sharafudeen R, Al-Hashim JM, Al-Harbi MO, Al-Ajwad AI, Al-Waheed AA. Preparation and Characterization of Precipitated Silica using Sodium Silicate Prepared from Saudi Arabian Desert Sand. Silicon. 2017;9(6):917-922. https://doi.org/10.1007/s12633-016-9531-8
33. Mohamed Ismail AA, Kannadasan K, Pichaimani P, Arumugam H, Muthukaruppan A. Synthesis and characterisation of sodium silicate from spent foundry sand: Effective route for waste utilisation. J Clean Prod. 2020;264:121689. https://doi.org/10.1016/j.jclepro.2020.121689
34. Joni IM, Rukiah R, Panatarani C. Synthesis of silica particles by precipitation method of sodium silicate: Effect of temperature, pH and mixing technique. AIP Conf Proc. 2020;2219:080018. https://doi.org/10.1063/5.0003074
35. Matinfar M, Nychka JA. A review of sodium silicate solutions: Structure, gelation, and syneresis. Adv Colloid Interface Sci. 2023;322:103036. https://doi.org/10.1016/j.cis.2023.103036
36. Novita L, Idris I. Effectiveness of silica gel from palm kernel shell ash as a moisture absorber of bottle packaging medicine. IOP Conf Ser Earth Environ Sci. 2022;1041:012044. https://doi.org/10.1088/1755-1315/1041/1/012044
37. Pisal A, Rao A. Comparative studies on the physical properties of TEOS, TMOS and Na2SiO3 based silica aerogels by ambient pressure drying method. J Porous Mater. 2016;23(6):1547-1555. https://doi.org/10.1007/s10934-016-0215-y
38. Meilani B, Shofiyani A, Wahyuni N. Synthesis of Red Mud-Based SiO2 with Various NaOH Concentrations and Extraction Times. Indones J Chem Sci. 2023;12(3):289-296.
39. Panwar K, Jassal M, Agrawal A. In situ synthesis of Ag-SiO2 Janus particles with epoxy functionality for textile applications. Particuology. 2015;19:107-112. https://doi.org/10.1016/j.partic.2014.06.007
40. Pérez Casas JA, Álvarez Mendez A, Ruiz Valdés JJ, Parra SD La, Zaldivar-Cadena AA, López Pérez D, et al. Sugarcane Bagasse Ash as an Alternative Source of Silicon Dioxide in Sodium Silicate Synthesis. Preprints. 2023;2023062233. https://doi.org/10.20944/preprints202306.2233.v1
41. Venkateswaran S, Yuvakkumar R, Rajendran V. Nano Silicon from Nano Silica Using Natural Resource (RHA) for Solar Cell Fabrication. Phosphorus Sulfur Silicon Relat Elem. 2013;188(9):1178-1193. https://doi.org/10.1080/10426507.2012.740106
42. Rubio F, Rubio J, Oteo J. A FT-IR study of the hydrolysis of Tetraethylorthosilicate (TEOS). Spectrosc Lett. 1998;31(1):199-219. https://doi.org/10.1080/00387019808006772
43. Ghasemi E, Ghahari M. Synthesis of Silica Coated Magnetic Nanoparticles. Int J Nanosci Nanotechnol. 2015;11(2):133-137.
44. Waseem M, Mustafa S, Naeem A, Shah K, Shah I, Ihsan-Ul-Haque. Synthesis and characterization of silica by sol-gel method. J Pak Mater Soc. 2009;3(1):19-21.
45. Dabbaghian MA, Babalou AA, Hadi P, Jannatdoust E. A Parametric Study of the Synthesis of Silica Nanoparticles via Sol-Gel Precipitation Method. Int J Nanosci Nanotechnol. 2010;6(2):104-113.
46. Deshmukh P, Bhatt J, Peshwe D. Determination of silica activity index and XRD, SEM and EDS studies of amorphous SiO2 extracted from rice husk ash. Trans Indian Inst Met. 2012;65(1):91-98. https://doi.org/10.1007/s12666-011-0071-z
47. Oktavia B, Ramadhani I, Zainul R. Synthesis of sodium silicate (Na2SiO3) from natural silica using sodium hydroxide (NaOH). J Chem. 2023. https://doi.org/10.1063/5.0125635
48. Deng J, Wu G, Xia Y, Liu L. Preparation and hydration properties of sodium silicate-activated municipal solid waste incineration bottom ash composite slag cementitious materials. J Mater Sci. 2024. https://doi.org/10.20944/preprints202404.1085.v1
49. Santos C, Dias C. Note on the coefficient of variation properties. Braz Electron J Math. 2021;2(4):101-111. https://doi.org/10.14393/BEJOM-v2-n4-2021-58062
50. Yeasmin MN, Sultana M, Siddika A, Tabassum S, Mahmud Ullah S, Bashar MS. Structural, Optical, and Morphological Characterization of Silica Nanoparticles Prepared by Sol-Gel Process. J Turk Chem Soc Sect A Chem. 2022;9(4):1323-1334. https://doi.org/10.18596/jotcsa.1071086
51. Rahman IA, Padavettan V. Synthesis of Silica Nanoparticles by Sol-Gel: Size-Dependent Properties, Surface Modification, and Applications in Silica-Polymer Nanocomposites-A Review. J Nanomater. 2012;2012:132424. https://doi.org/10.1155/2012/132424
52. Owoeye SS, Abegunde SM, Oji B. Effects of process variable on synthesis and characterization of amorphous silica nanoparticles using sodium silicate solutions as precursor by

sol-gel method. Nano-Struct Nano-Objects. 2021;25:100625. https://doi.org/10.1016/j.nanoso.2020.100625
53. Zulfiqar U, Subhani T, Wilayat Husain S. Synthesis of silica nanoparticles from sodium silicate under alkaline conditions. J Solgel Sci Technol. 2016;77(3):753-758. https://doi.org/10.1007/s10971-015-3950-7
54. Yuan M, Lu J, Kong G. Effect of SiO2:Na2O molar ratio of sodium silicate on the corrosion resistance of silicate conversion coatings. Surf Coat Technol. 2010;204(8):1229-1235. https://doi.org/10.1016/j.surfcoat.2009.10.024
55. Mekki A, Holland D, McConville CF, Salim M. An XPS study of iron sodium silicate glass surfaces. J Non Cryst Solids. 1996;208(3):267-276. https://doi.org/10.1016/S0022-3093(96)00523-6
56. Jensen DS, Kanyal SS, Madaan N, Vail MA, Dadson AE, Engelhard MH, et al. Silicon (100)/SiO2 by XPS. Surf Sci Spectra. 2013;20(1):36-42. https://doi.org/10.1116/11.20121101
57. Najafi A, Ghasemi S. A study of APC surfactant role on the surface characteristics, size and morphology improvements of synthesized mesoporous silica nanopowder through a sol-gel process. J Alloys Compd. 2017;720:423-431. https://doi.org/10.1016/j.jallcom.2017.05.274
58. Tang C, Zhu J, Zhou Q, Wei J, Zhu R, He H. Surface Heterogeneity of SiO2 Polymorphs: An XPS Investigation of α-Quartz and α-Cristobalite. J Phys Chem C. 2014;118(45):26249-26257. https://doi.org/10.1021/jp509338x
59. Zou J, Dai Y, Pan K, Jiang B, Tian C, Tian G, et al. Recovery of silicon from sewage sludge for production of high-purity nano-SiO2. Chemosphere. 2013;90(8):2332-2339. https://doi.org/10.1016/j.chemosphere.2012.10.087